X-band weather radar monitoring of precipitation fields in Naples urban areas: data quality, comparison and analysis

Vincenzo Capozzi[1], Errico Picciotti[2], Giorgio Budillon[1,3], Frank S. Marzano[4]

[1]Università degli studi di Napoli "Parthenope" (Italy), [2]CETEMPS – Università dell'Aquila (Italy)
[3]CINFAI – Consorzio Interuniversitario Nazionale per la Fisica delle Atmosfere e delle Idrosfere
[4]Dipartimento di Ingegneria dell'Informazione, Sapienza Università di Roma (Italy)
(Dated: 17 July 2014)

Vincenzo Capozzi

1 Introduction

Rain gauges are considered a traditional method for measuring rainfall. They are simpler than weather radar in terms of management, but they can only provide point measurements and offer limited information on spatial rainfall variability (e.g., Borga and Tonelli, 2002; Steiner et al., 2009). To capture the spatial variability of storms over relatively large areas, weather radars are needed (Battan, 1973; Doviak and Zrnic, 1993). Usually, the costs of installation and maintenance these systems are one of the main limitations for their diffusion. Recently, the increased use of X band frequencies for weather radar applications, for instance to cover small catchments and urban areas, has pushed the activity to develop, improve and study such systems (e.g., Delrieu et al., 1999b; Maki et al., 2005; Marzano et al., 2010; Picciotti et al., 2013).

In this respect, since November 2011, a single polarization X-band weather radar, called WR-10X, has been installed in Naples' urban area at the top of Castel Sant'Elmo (280 m a.s.l.). The radar belongs to the Campania Center for Marine and Atmospheric Modelling and Monitoring (CCMMMA) of the University of Naples "Parthenope" and provides high resolution rainfall data which are necessary for monitoring urban flash flood and for runoff simulation in urban drainage.

The objective of this work is to calibrate WR-10X rain-rate estimation with the available rain-gauge network using time-space correlation approach in according to rainfall nature (stratiform, convective and mixed). To mitigate ground and sea clutter returns, path attenuation and other impairments, a processing chain has been applied to radar data before rain-rate estimation. To pursue this aim, a large set of data covering a two years period and consisting of radar scans and gauge measurements, have been collected and carefully processed. The structure of the article will follow the list of the topics just mentioned.

2 Weather radar system

WR-10X weather radar of CCMMMA, installed in Naples, is a single-polarization system manufactured by ELDES srl. In operative mode WR-10X scanned in a 360° sector and for 1°, 2°, 3°, 4°, 5° and 10° elevation elevations angles; the three upper elevation angles were selected to avoid ground clutter and beam blockage in some direction of scan horizon. The pulse repetition frequency is 800 Hz with 300 m range resolution (gate length). The parabolic type dish antenna is very compact and is characterized by a pencil-beam of about 3 degrees. Antenna rotation rate is 20 °/s and the time period for a full volume scan is about 3 minutes (with 6 elevations). Some radar operational products have been developed by HIMET srl to enhance the monitoring potentiality of WR-10X. The main characteristics and installation facility of WR-10X are given in Fig. 1.

Manufacturer	ELDES
Location	Napoli Castel Sant'Elmo (40.8438°N 14.2385°E)
Height (a.s.l.)	280 m
Frequency	9.4 GHz
PRF	800 Hz
Available Range	36 and 72 km
Beamwidth	3.0
Peak power	10 kW
Angolar resolution	3° azimuth
Range resolution	300 m

Figure 1: Main technical characteristics of WR-10X weather radar (left panel) and radar installation at Castel Sant'Elmo in Naples (right panel).

3 Processing chain to overcome systematic error

Rainfall estimation errors by weather radars can be grouped in two main categories (e.g., Borga and Tonelli, 2002): systematic and random errors. Systematic errors include biases and range dependent effects. The main source of bias errors includes drifts in radar calibration constant and systematic variations in the relationship between radar reflectivity and rain-rate. For range-dependent errors, they are caused mainly by the scan geometry of weather radars, the variations in the reflectivity profile, the attenuation by rain and partial beam filling. On the other hand, random errors could originate from the variability of rainfall within the resolution cell and radar hardware system noise. The presence of complex orography introduces amplification effects for some of these errors.

In this section an analysis of systematic errors is dealt with, focused our attention to:

- Ground clutter residuals;

- Backscatter from sea surface (sea clutter);

- Beam attenuation along the path.

3.1 Ground clutter residuals

The methodologies aimed at the identification and removal of clutter echoes are based on some features with which this noise manifests itself, such as zero velocity and low spectral amplitudes (Doviak and Zrnic, 1993). Ground clutter is often associated to a field reflectivity typically much more textured than that of precipitation (Nicol et al., 2011). In the WR-10X radar a statistical declutter filter is implemented, based on the different samples distribution between clutter echoes and meteorological echoes. This filtering procedure could be improved by means of a statistical filter in order to eliminate the residual noise generated by ground clutter. The statistical filter is based on three main ingredients:

1) Entropy calculation. This step is used to recognize the radar map which deserves a filtering;

2) Texture calculations. Spatial texture basically describes the local variance of the input field. Usually high variance is associated to non-meteorological echoes;

3) Median filtering. This step is applied on a Boolean mask instead of directly to the input field. This step is used to cutting out residuals spikes.

The methodology has been modulated in the context of this work through the analysis of multiple cases studies, related to low and high rainfall events. The choice of threshold on local variance is particularly critical: the performed analysis has suggested to adopt a lower threshold in the closer range, where the residual noise frequently occurs, and, in general, when super refraction atmospheric conditions occur. In Fig. 2a and Fig. 2b, unfiltered and filtered VMI maps for a high rainfall event are shown.
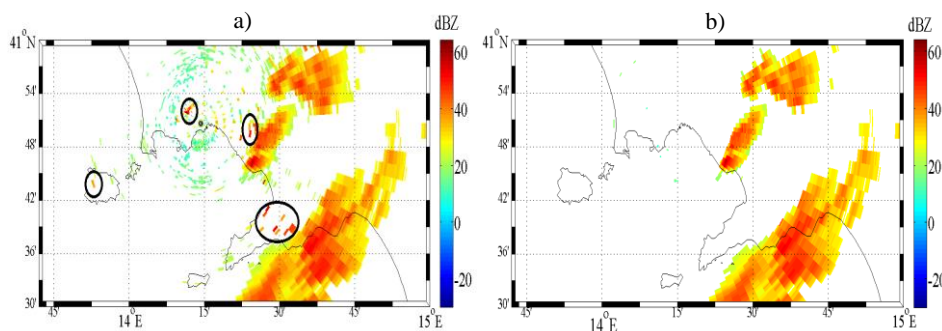

Figure 2: (a) VMI reflectivity map acquired on October 27, 2012 at 14:25 UTC. The zoom on Naples Gulf emphasizes the presence of ground clutter residues, whose most important evidence are indicate by black circles. (b) The same map, but with ground clutter residues correction.

3.2 Backscatter from sea surface

This phenomenon occurs during rough sea conditions when radar beam interacts with the sea waves or sea sprays and can be compounded when super refractions conditions occur. Sea clutter is characterized by low reflectivity values, by a slightly grainy texture and echoes generally persistent in location and intensity. The approach we used to suppress sea clutter noise is based on vertical reflectivity profile analysis (Alberoni et al. 2001): in rainy conditions usually vertical reflectivity profiles are smooth and regular, while in sea clutter condition a broken profile is often observed. The approach starts with vertical difference reflectivity analysis:

$$RD = Z_1 - Z_2 \qquad\qquad (3.1)$$

where Z_1 and Z_2 are reflectivity measurements at two different antenna elevation angles above the same terrain point. A careful analysis of PPI at the lowest elevation angles showed the occurrence of sea clutter only at 1°; thus we compute RD using reflectivity data measured at 1° (Z_1) and 2° (Z_2) antenna elevation angles. Sea clutter echoes are diagnosed when one of the following conditions occur:

$$\text{(a)} \quad RD > T_1 \tag{3.2}$$

$$\text{(b)} \quad RD > 0 \ \& \ Z_2 < T_2 \tag{3.3}$$

where T_1 and T_2 are empirical threshold values. The filter has been tested in several case studies, a nice example of application is shown in Fig. 3 related to a 13/01/2013 event, when both meteorological and non-meteorological echoes were detected in the Gulf of Naples.
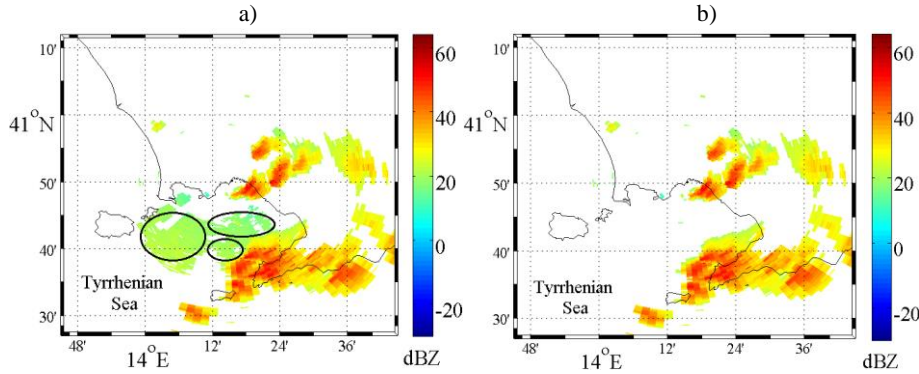

Figure 3: (a) VMI reflectivity map acquired on January 13, 2013 at 14:55 UTC, affected by sea clutter. The sea clutter in the Gulf of Naples is highlighted by black circles. (b) The same map, after sea clutter correction procedure.

3.3 Beam attenuation along the path

It is well know that electromagnetic energy incident on a target (atmospheric gases, clouds and hydrometeors) is subjected both to scattering and absorption. The radar beam power is reduced by a factor that depends on medium type, medium density and electromagnetic wave frequency. This issue has a significant relevance at X-band (e.g. Delrieu et al. 1999 a,b) and it is strongly dependent on rain rate (Marzano et al. 2003). Attenuation coefficient (k, dB/km) and reflectivity factor (Z, mm⁶ m⁻³)

Attenuation coefficient (k, dB/km) and reflectivity factor (Z, $mm^6 \ m^{-3}$) are typically related by a power law:

$$k = \alpha Z^{\beta} \tag{3.4}$$

The two-way attenuation between two radar cells adjacent in range ($A_{(i-1,i)}$) can be computed by means of Eq. 3.5, in which L is the radar bin resolution (0.3 km in our case) and Z_i the non-corrected reflectivity (measured) in the i-cell.

$$A_{(i-1,i)} = 2L \ k = 2L \ \alpha Z_i^{\beta} \tag{3.5}$$

The literature offers many choices for α and β values: Battan (1973) suggests $(\alpha, \beta) = (0.00029, 0.72)$, Perez and Zawadzki (2003) suggest (0.000372, 0.72), while Delrieu et al. (1997) provide $0.75 \leq \beta \leq 0.85$ on the basis of an empirical approach. In this work we try to mitigate attenuation issue with an iterative procedure that involves the estimation of the two-way path integrated attenuation (PIA) along the entire beam path. PIA, integrated from the radar-site to the cell i-1, can be obtained according to the formula:

$$PIA_{(0,i-1)} = \sum_{j=1}^{i-1} A_{(j-1,j)} \tag{3.6}$$

From Z_i, the corrected reflectivity $Z_{corr(i)}$ in i-cell can be computed according to:

$$Z_{corr(i)} = Z_i 10^{\frac{PIA(0,i-1)+A(i-1,i)}{10}} \tag{3.7}$$

The attenuation has been computed adopting α and β proposed by Perez and Zawadzki (2003). The algorithm just described has been tested for moderate rainfall events in which attenuation problem can be of particular relevance. An example of results is shown in Fig. 4, related to the event occurred on 17/12/2012. The inherent divergence of the proposed iterative algorithm is known to be an issue for convective rainfall high intensities due to the amplification of small initial errors (Delrieu et al., 1999b; Marzano et al., 2003); in this respect a maximum threshold of PIA is set to avoid unrealistic values.
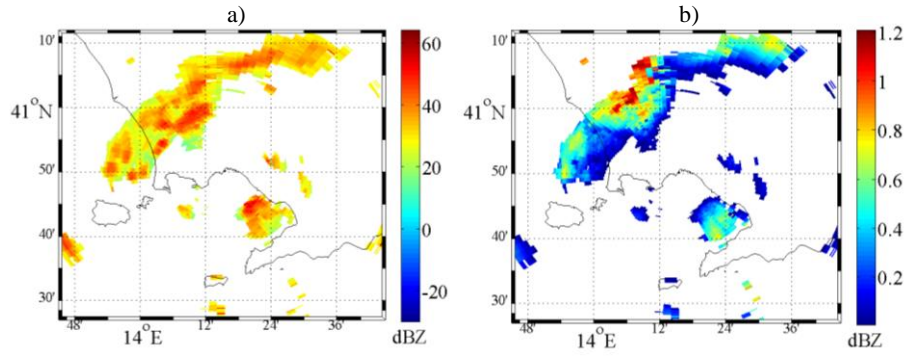
Figure 4: (a) Attenuated reflectivity map (VMI) acquired on December 17, 2012 at 16:55 UTC and (b) corresponding attenuation compensation map obtained through the PIA iterative correction method.

4 Raingauge-based calibration of radar rainfall estimation

In order to perform a raingauge-based calibration of quantitative precipitation estimates (QPE) provided by WR-10X, we follow various steps. In the first step, after applying all correction procedure described in previous section, reflectivity factor Z (in dBZ) was resampled from original spherical coordinates (r, θ, φ) to uniform 2-D Cartesian grid (x-axis integer i, y-axis integer j), having 0.3 km step, at each radar acquisition time t (the radar volume time step is 5 minutes), selecting VMI(r, θ, φ) for each (i,j). In order to mitigate the undesirable effect of hail, we used a maximum threshold reflectivity ("hail cap") of 53 dBZ.

As a second step, the radar reflectivity field has been classified into stratiform and convective rainfall using the technique developed by Steiner et al. (1995); the aforementioned method has been slightly modified for preserving results by residues reflectivity spikes. More specifically, radar pixel classified as convective rain has been compared with the surrounding background: if its intensity exceeds a selected threshold (given by the sum of average intensity and standard deviation of the surrounding background), it is treated as a spike and its reflectivity value has been replaced with the surrounding background average intensity.

As a third step, the VMI product has been converted into radar-estimated rain-rate R(i,j,t) (in mm/h) using the following estimator:

$$R(i,j,t) = \left(10^{\frac{Z(i,j,t)}{10}}\right)^{\frac{1}{b}}\left(\frac{1}{a}\right) \tag{4.1}$$

where the regression coefficients are for the X-band radar (Maki et al. 2005):

$$\begin{cases} a = 348, b = 181 \ for \ stratiform \ rain \\ a = 134, b = 1.55 \ for \ convective \ rain \end{cases}$$

In the fourth step, rain rate maps has been linearly interpolate, in order to fill any gaps in radar volume time series. Finally, the rain rate field has been converted in cumulative rainfall, assuming that rain field is stationary in space and intensity between two consecutive scans (Fabry et al. 1994); the integration time interval chosen for the analysis is 24 hour. To reduce spatial mismatching effects, we have considered the nine pixels closer to rain-gauge location (i_g,j_g) and we selected among these the pixel with 24-h cumulative rainfall value $R(i_g,j_g)$ closest to that reported by in-situ measurements. If $G(i_g,j_g)$ is a rain-gauge 24-h cumulative rainfall measure at each (i_g,j_g), the gauge-to-radar cumulative rainfall ratio factor F_{ij} is defined by:

$$F_{ij} = \frac{G(i_g,j_g)}{R(i_g,j_g)} \tag{4.2}$$

In order to evaluate the goodness of radar QPE through the comparison with rain-gauge data, we have performed a statistical analysis. After introducing the absolute error $ERR = R(i_g,j_g) - G(i_g,j_g)$ and indicating with angle brackets the ensemble averaging and with bars the absolute value, we have used the following indexes: i) $BIAS = \langle ERR \rangle$; ii) the absolute mean error $D = \langle |ERR| \rangle$; iii) the root mean square error $RMSE = \sqrt{\langle (ERR)^2 \rangle}$, whose optimal value is 0; iv) the mean field ratio bias $MRB = \frac{\langle R \rangle}{\langle G \rangle}$, whose optimal value is 1; v) the fractional standard error $FSE = \frac{\sqrt{\langle (ERR)^2 \rangle}}{\langle G \rangle}$, whose optimal value is 0.

The study of F variability in range has been carried out through an exponential model, in order to define a correction factor that is dependent from the distance of the radar-site. The adoption of this approach is suggested by conical scanning peculiarities, which may determine an underestimation of surface rain field due to the increasing height of the sampled atmospheric volume (Picciotti et al. 2008). Moreover, because of orographic features, an underestimation of rainfall in the eastern and southeastern azimuth is expected. The exponential dependence on the range $r(i_g,j_g)$ between the radar and the each rain-gauge at the location (i_g,j_g) can be developed using the following exponential factor F_{ER}:

$$F_{ER} = a_e e^{b_e r(i_g, j_g)} \qquad\qquad (4.3)$$

with a_e and b_e proper regression coefficients, derived by the spatial ensemble of available data. Then the calibrated rain estimation is given by:

$$\hat{R}(i,j) = F_{ER}[r(i,j)]R(i,j) \qquad\qquad (4.4)$$

where R(i,j) is non-calibrated rain estimation.

Rain gauge and radar estimations, concerning 15 storms and covering a variety of synoptic features and precipitation patterns between April and December 2012, have been taken into account for this analysis. The type of rainfall events has been determined means of a synoptic analysis and using information provided by Steiner's precipitation type recognition technique. The results obtained suggested to subdivide precipitation events into three categories: i) "Mainly stratiform events"; ii) "Mainly convective events" and iii) "Mixed events". The latter category includes those events whose nature is uncertain, due to the simultaneous presence of both stratiform rain and embedded convection. Such events are particularly frequent in the study area, especially in late autumn, in winter and in early spring and they are often associated to the passage of an occluded front.

The statistical results for all events analyzed, in terms of accumulated rain over the whole area on a time interval of 24 hours, has showed that weather radar tends generally to underestimate surface rainfall, as highlighted by BIAS sign, which is negative for all events. Radar underestimation becomes particularly significant for the stratiform events, while tends to reduce when mixed and convective cases are considered. The analysis of radar QPE maps showed that a strong bright band effect often occurs in stratiform and in mixed events. This phenomenon is quite evident on VMI map in terms of a circular or arcing band of higher reflectivity values, and, consequently, can lead to an overestimation of QPE in the closer range. However, when moderate and persistent rainfall occurs, that is a typical feature of warm front associated to stratiform events, the attenuation can be particularly severe and, in combination with orographic beam-blocking, can develop a strong underestimation at the further range or, in some extreme cases, a radar-failure in detecting rainfall. Radar QPE underestimation in weak reflectivity gradient events (stratiform precipitation) is documented by many studies that have compared radar and rain-gauge derived rainfall (e.g. Klazura et al. 1999; Stellman et al. 2001). This issue might be tackled by correcting for the bright band effects due to the snow melting layer in stratiform rain (Marzano et al., 2004).

In order to take into account the dependence of rainfall type, we have decided to introduce three exponential models: for the stratiform events, the best fit is achieved when a_e=0.2272, b_e=0.0970, for the convective events when a_e=0.6445, b_e=0.0408, for the mixed events when a_e=0.2775, b_e=0.0721. The behavior of F with respect to radar range for all events considered is shown in Fig. 5. Stratiform and mixed models have a similar behavior in the first 15 km, then they reveal significant differences. Convective model exhibits a different behavior from the other two both at the further range, in which radar underestimates are less important, and at the closer range, in which radar QPE are generally more in agreement with rain-gauge data for this type of events.
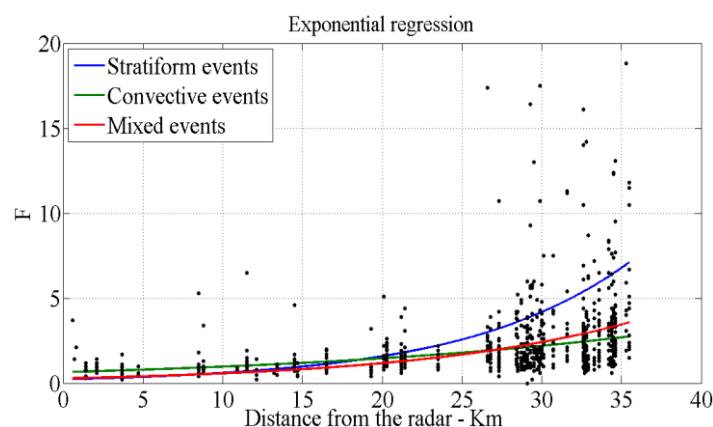

Figure 5: Exponential correction factor as function of radar range. Blue line represents the exponential regression for stratiform events, red line the exponential regression for mixed events and the green line that for the convective events.

5 Application to case study on November 30, 2012

In order to perform a robust calibration, we have tested the exponential regressions on several rain events not belonging to the dataset used to derive the factor F.

An example of application can be seen on November 30, 2012 event, when Campania Region has been affected by a moderate and unstable south-western flow, triggered by a low-pressure system located over the high Tyrrhenian sector. In this event convective precipitation prevailed in the night and during the morning, while stratiform contributions were predominant in the early afternoon thus leading to a mixed event classification. A large regional network of remotely-operated rain gauges

is available in Campania Region as a merge of several networks; as shown in Fig. 6, in the area covered by weather radar about 50 rain-gauges are accessible every 10 minutes.
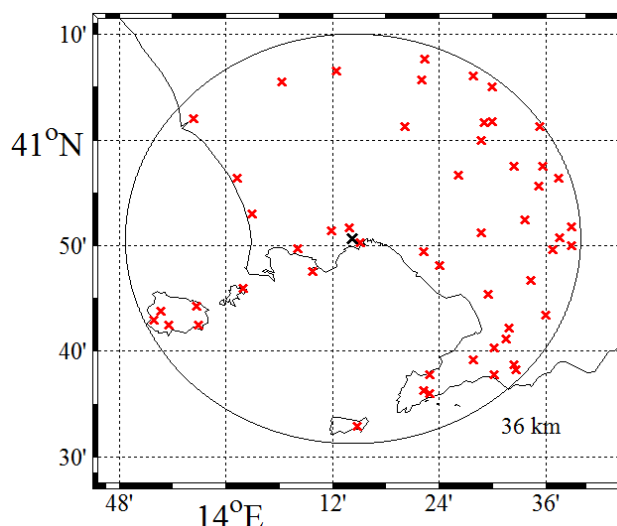

Figure 6: Map of study region including radar location (black cross) and raingauge network (red crosses). Circular line at 36 km far from Napoli Castel Sant'Elmo indicate the limit of the region used for results analysis.

The distribution of 24-hours rainfall amount (see Fig. 7a) from 00:00 UTC 30 November 2012, provided by a natural neighbor interpolation of rain gauge data, shows higher values in the Vesuvio area, in the Sorrentine Peninsula and generally in the inland sectors. In the north-western azimuth scarce rainfall values were recorded instead. WR-10X rainfall estimates (Fig. 7b) show an overestimation in the closer range, due in part to the bright band effect and in part to the presence of hail and other solid hydrometeors in the convective systems.

A strong underestimation is quite evident at further range in the eastern and south-eastern sectors. By adopting the adjustment factor in Eq. (4.4), we have calibrated the radar rain estimation using the proper coefficients for mixed events. The effect of correction factor F is apparent by looking at Fig. 7c. The improvements are particularly considerable in the areas where maxima rainfall amounts were detected, although local underestimates still remain; such areas coincide with those in which radar beam is partially blocked by orography. The statistical analysis, for the whole event, is summarized in Table 1: the introduction of a corrective distance factor resolves in better scores for all statistical indexes.
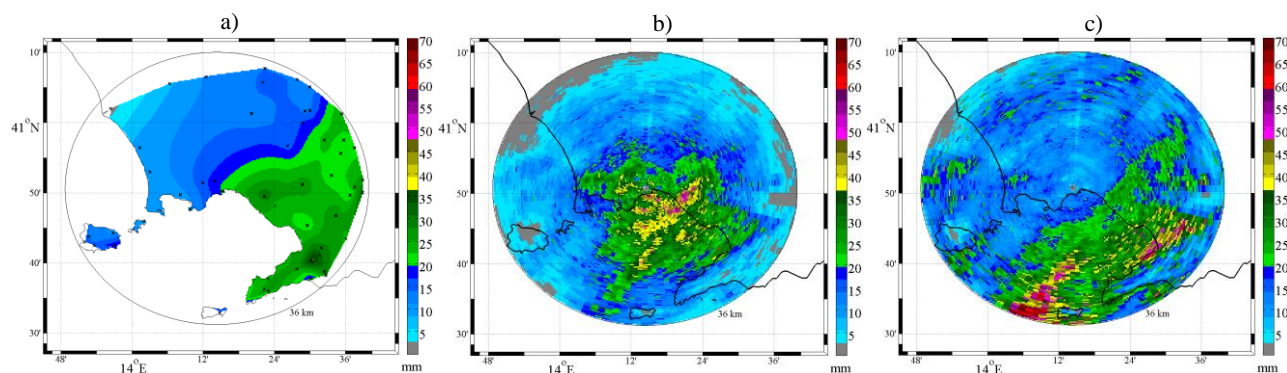

Figure 7: (a) Daily interpolated accumulated rainfall derived from the rain-gauge network (black circles) on November 30, 2012. (b) Radar-derived QPE for the same event and (c) the impact of distance factor F(r) on radar estimation. The accumulated rainfall is color-coded according to the vertical bar (in mm).

Table 1: Statistical scores of 24-h radar surface rainfall estimates before and after the calibration procedure for the test on 30 November, 2012.

Statistical score	by using $R(i,j)$	by using $\hat{R}(i,j) = F_{ER}[r(i,j)]R(i,j)$
BIAS	-9.1	-2.0
D	10.7	6.2
RMSE	12.9	8.3
MRB	0.52	0.89
FSE	0.67	0.43

Conclusions

One of the challenges in the near future radar meteorology is to exploit the advantage of X-band systems, which allow the design of small-size compact instruments and the delivery of low-cost portable systems with relatively high performance. In this respect a highly-sophisticated X-band single-polarization prototype has been installed and tested since November 2011 at the top of Castel Sant'Elmo in Naples in the south of Italy.

The aims of this work were to develop some quality control procedures for X-band weather radar reflectivity measurements and to perform a raingauge-based calibration technique. The use of radar with high frequency (i.e. X-band) has proven particularly useful for mitigating some of the limitation of traditional operational systems, by exploiting the benefit of easiness to transport and deploy and the reduced cost for maintenance. The drawback is that X-band signals may be heavily attenuated in intense rainfall and hail, such as what found in convective systems. The correction procedure implemented aiming at mitigate this issue, using the PIA iterative method, is rather inadequate when these circumstances occur. Therefore, future work shall be devoted to improve beam attenuation correction, exploring new strategies, involving, for example, the use of ground clutter echoes at lowest antenna elevation angles (Delrieu et al. 1997, 1999a,b).

Rain estimation from WR-10X has been compared with network gauges measurement over several events. As general result we note a strong underestimation with increasing distance from radar, particularly when stratiform or mixed rainfall events occur. To overcome this problem, a calibration technique based on exponential regression has been trained for three prevailing rainfall type (stratiform, convective and mixed) on a dataset consisting of 15 events. The proposed method has been tested for a mixed rainfall event occurred on November 30, 2012. The results highlighted a strong BIAS reduction and an improvement in all statistical scores considered. However, to improve our results, in the future we will focus our attention to assess a calibration methodology using a correction factor dependent on both range and azimuth. Nevertheless, because of the great variability in the intensity and distribution of rainfall, more radar-gauge intercomparisons should be carried out to cover a larger number of rainfall events.

Finally, it should be noted that, even though the outlined calibration procedure is purely empirical, it could have a significant impact on activities related to civil protection alarming and to urban flash-flood prevention actions.

Acknowledgement

References

Alberoni, P. P., Andersson, T., Mezzasalma, P., Michelson, D. B., and Nanni, S., Use of the vertical Reflectivity profile for Identification of Anomalous propagation, Meteorol. Appl., 2001, Vol. 8 (3), pp. 257 – 266.

Battan L. J., Radar Observation of the Atmosphere, University of Chicago Press, 1973, 324 pp.

Borga, M., and Tonelli, F., 2002, Long-term assessment of bias adjustment in radar rainfall estimation, Water Resources Research, vol. 38, 11, 1226.

Delrieu, G., Caoudal, S., and Creutin, J.D., Feasibility of using mountain return for the correction of ground-based X-band weather radar data, J. Atmos. Oceanic Technol., 1997, Vol. 14, pp. 367–385.

Delrieu, G., Hucke, L., and Creutin, J.D., Attenuation in Rain for X- and C-Band Weather Radar Systems: Sensitivity with respect to the Drop Size Distribution, Journal of Applied Meteorology, 1999a, Vol. 38, pp. 57-68.

Delrieu, G., Serrar, S., Guardo, E., and Creutin, J.D., Rain Measurement in Hilly Terrain with X-Band Weather Radar Systems: Accuracy of Path-Integrated Attenuation Estimates Derived from Mountain Returns, J. Atmos. Oceanic Technol., 1999b, Vol. 16, pp. 405–416.

Doviak, R., and Zrnic, D., Doppler radar and weather observations, Academic Press UK, 1993, pp. 592.

Fabry, F., Bellon, A., Duncan M.R., and Austin, G.L., "High resolution rainfall measurements by radar for very small basins: the sampling problem re-examined", 1994, J. Hydrol., Vol. 116, pp. 415-28.

Germann U., and Joss, J., Operational measurement of precipitation in mountainous terrain, Advanced Applications of weather radar, P. Meischner, Ed. Heidelberg, Germany: Springer-Verlag, 1999, Vol. 13, pp. 1025-1043.

Klazura, G.F., Thomale J., Kelly, D., and Jendrowski, P., A comparison of NEXRAD WSR-88D rain estimates with gauge measurements for high and low reflectivity gradient precipitation events. Preprints, 29th Int. Conf. on Radar Meteorology, Montreal, PQ, Canada, Amer. Meteor. Soc., 1999, pp. 722-725.

Maki, M., Park, S.G., and Bringi, V.N., Effect on natural in rain drop size distributions on rain rate estimations of 3 cm wavelength polarimetric radar, Journal Meteorological Society of Japan, 2005, Vol. 83, No 5, pp 871-893.

Marzano, F.S., Roberti, L., Di Michele, S., Tassa, A., and Mugnai, A., Modeling of apparent radar reflectivity due to convective clouds at attenuating wavelengths, Radio Sci., 2003, Vol. 38, No. 1, 1002.

Marzano, F.S., Picciotti, E., and Vulpiani, G., Rain field and reflectivity vertical profile reconstruction from C-band radar volumetric data, IEEE Trans. Geosci. Rem. Sens., 2004, Vol. 42, No.4, pp. 1033-1046.

Nicol, J.C., Illingworth, A.J., Darlington, T., and Sugier, J., Techniques for improving ground clutter identification, Weather radar hydrology: proceedings of a symposium held in Exeter, UK, April 2011, IAHS Publ. 3XX, 2011.

Perez, M.A., and Zawadzki, I., S- and X-band dual-wavelength radars revisited, Preprints, 31st Int. Conf. on Radar Meteorology, Seattle, WA, Amer. Meteor. Soc., 2003, pp. 51–54.

Picciotti, E., Gallese, B., Cimoroni, A., Montopoli, M., Telleschi, A., Volpi, A., Consalvi, F., Cinque, G., and Marzano, F.S., C-band radar precipitation measurements in mountainous region: comparison with raingauge fields and X-band radar data, Proceedings of ERAD 2008 – The Fifth European Conference on Radar in Meteorology and Hydrology, 2008.

Steiner, M., Houze, R.A., and Yuter, S.E., Climatological Characterization of Three-Dimensional Storm Structure from Operational Radar and Rain Gauge Data, J. Appl. Meteor., 1995, Vol. 34, pp. 1978–2007.

Steiner, M., Smith, J.A., Burges, S.J., Alonso, C.V., and Darden, R.W., Effect of bias adjustment and rain gauge data quality control on radar rainfall estimation, Water Resources Research, 1999, Vol. 35 (8), pp. 2487-2503.

Steiner, M., and Smith, J.A., Use of Three-Dimensional Reflectivity Structure for Automated Detection and Removal of Nonprecipitating Echoes in Radar Data, J. Atmos. Oceanic Technol., 2002, Vol. 19, pp. 673–686.

Stellman, K.M., Fuelberg, H.E., Garza, R., and Mullusky, M., An examination of Radar and Rain Gauge-Derived Mean Areal Precipitation over Georgia Watersheds, American Meteorological Society, 2001, Vol. 16, pp 133-144.